Journal of The Electrochemical Society, **150** (7) A905-A911 (2003)
0013-4651/2003/150(7)/A905/7/$7.00 © The Electrochemical Society, Inc.

Study of Mn Dissolution from $LiMn_2O_4$ Spinel Electrodes Using Rotating Ring-Disk Collection Experiments

Li-Fang Wang,[a] Chin-Ching Ou,[a] Kathryn A. Striebel,[b,*] and Jenn-Shing Chen[c,*,z]

[a]*School of Chemistry, Kaohsiung Medical University, Kaohsiung, Taiwan 807*
[b]*Lawrence Berkeley National Laboratory, University of California, Berkeley, California 94720, USA*
[c]*Department of Chemical Engineering, I-Shou University, Kaohsiung, Taiwan 840*

The goal of this research was to measure Mn dissolution from a thin porous spinel $LiMn_2O_4$ electrode by rotating ring-disk collection experiments. The amount of Mn dissolution from the spinel $LiMn_2O_4$ electrode under various conditions was detected by potential step chronoamperometry. The concentration of dissolved Mn was found to increase with increasing cycle numbers and elevated temperature. The dissolved Mn was not dependent on disk rotation speed, which indicated that the Mn dissolution from the disk was under reaction control. The *in situ* monitoring of Mn dissolution from the spinel was carried out under various conditions. The ring currents exhibited maxima corresponding to the end-of-charge (EOC) and end-of-discharge (EOD), with the largest peak at EOC. The results suggest that the dissolution of Mn from spinel $LiMn_2O_4$ occurs during charge/discharge cycling, especially in a charged state (at >4.1 V) and in a discharged state (at <3.1 V). The largest peak at EOC demonstrated that Mn dissolution took place mainly at the top of charge. At elevated temperatures, the ring cathodic currents were larger due to the increase of Mn dissolution rate.
 [DOI: 10.1149/1.1577543]

Manuscript submitted August 21, 2002; revised manuscript received January 13, 2003. Available electronically May 16, 2003.

The rapid progress in development and widespread use of portable electronic devices have led to a great demand for portable, lightweight power sources. Lithium-ion technology has met these requirements, and has been used commercially for over ten years because it offers high energy and power density, high voltage, long-life, and reliability. The performance of lithium-ion batteries is to a large degree determined by the cathode material. There have been many studies of the cathode materials during the last decade. Although $LiCoO_2$ has been widely used as the cathode material in the commercial lithium-ion batteries for many years, the lithium manganese oxide spinel $LiMn_2O_4$ is a promising alternative cathode material in the future because of its high voltage, low cost, and environmental friendliness. These attractive characteristics make spinel $LiMn_2O_4$ a good candidate for large-scale Li-ion batteries for electric vehicle (EV) and hybrid electric vehicle (HEV) applications.[1] However, capacity fading during charge/discharge cycling is a problem for the spinel, particularly at elevated temperatures. Several factors have been proposed to contribute to the capacity fading such as (*i*) the electrochemical reaction with the electrolyte at high voltage,[2,3] (*ii*) manganese dissolution into the electrolyte due to acid attack and a disproportion reaction at the particle surface[4-7] $\langle 2Mn_{(solid)}3+ \rightarrow Mn^{4+}_{(solid)} + Mn^{2+}_{(solution)}\rangle$ (*iii*) instability of the two-phase structure in the charged state leading to the loss of MnO and dissolution of Mn to a more stable single-phase structure,[4,8,9] (*iv*) formation of tetragonal $Li_2Mn_2O_4$ on the surface of the spinel and the associated Jahn-Teller distortion at the end of discharge, especially under high current density, nonequilibrium conditions,[5,10,11] (*v*) formation of oxygen-deficient spinels,[12] (*vi*) cation mixing between the lithium and manganese sites in the spinel lattice,[13] and (*vii*) loss of crystallinity during cycling.[14,15]

Although many possible factors have been proposed to contribute to the capacity fading of the spinel $LiMn_2O_4$ electrode, most of the evidence reported so far points to manganese dissolution at the top of charge as the major reason for the capacity fading. It is essential to investigate the dissolution behavior of the spinel electrode in order to improve the capacity fading of the spinel materials. The measurement of Mn concentration in the electrolyte solution is very important to understand the dissolution behavior of the spinel electrode. There have been many papers describing the measurement of the variation of the manganese concentration in the electrolyte during the charge-discharge process.[4,6,7,14,16-19] Although many chemical analysis techniques were applied to the quantitative analyses of Mn such as atomic absorption spectroscopy (AAS), inductively coupled plasma-atomic emission spectroscopy (ICP-AES), differential pulse polarography, and total reflection X-ray fluorescence (TXRF), only a few *in situ* techniques were applied to measure the Mn dissolution. Recently, Terada *et al.* monitored the concentration of Mn in an electrolyte solution during the electrochemical cycling by *in situ* methods using a combination of TXRF analysis and a capillary technique.[18] The rotating ring-disk electrode (RRDE) technique is another useful *in situ* technique to measure the Mn dissolution of the spinel $LiMn_2O_4$ electrode. In this work, the Mn dissolution behavior of the spinel electrode has been first explored by the RRDE technique. The RRDE was developed about forty years ago and has proved to be an invaluable tool for the study of electrochemical reactions. The RRDE consists of two concentric electrodes (disk and ring electrodes) in a cylindrical holder with both the electrodes facing downward into the solution. Products generated at the disk reaction are swept outward by the convection caused by rotation, and can be detected electrochemically at the ring by fixing a potential on the ring electrode. In this study, a disk electrode coated with the spinel $LiMn_2O_4$ materials and the Pt ring electrode was fixed at a $Mn^{2+}/Mn_{(s)}$ reduction potential to collect the dissolved Mn^{2+} ions in electrolytes. Although several different types of experiments are possible at the RRDE, rotating ring-disk collection experiments (RRCEs) and stripping voltammetry (SV) were used to detect manganese ions generated by the dissolution of the spinel cathode into the electrolyte at various reaction conditions in our experiments. The Mn dissolution from spinel was measured *in situ* under various conditions. Effects of cycle number, temperature, overcharge, and overdischarge on the spinel $LiMn_2O_4$ electrodes were investigated. Measurements of dissolved Mn^{2+} ions from the RRCEs were compared with those from the inductively coupled plasma-mass spectrometer (ICP-MS). Through this research, we could further understand the Mn dissolution behavior of the spinel electrode and the variation of manganese concentration in the electrolyte during the charge-discharge process.

Experimental

Fabrication of composite disk cathode.—Composite disk cathodes were prepared by wet coating. The composite disk cathodes were made from stoichometric spinel $LiMn_2O_4$ (EM Merck), acetylene black, SFG-6 (Timcal), and polyvinylidene fluoride (PVDF) binder (MKB-212C, Elf Atochem) in a weight ratio of 86:2:4:6. The

* Electrochemical Society Active Member.
z E-mail: jschen@isu.edu.tw

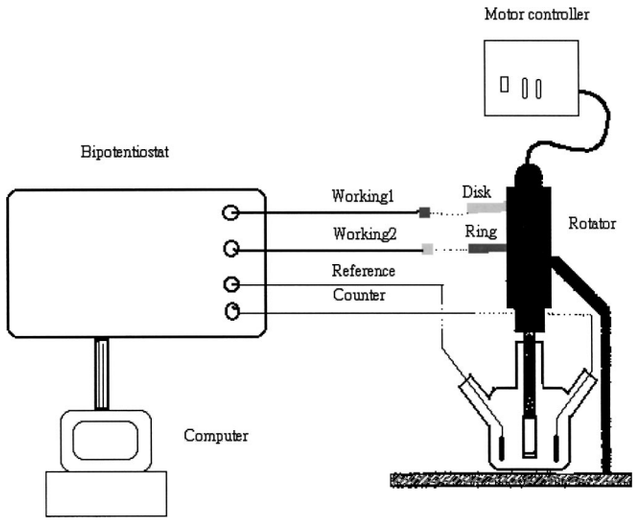

Figure 1. Schematic illustration of a four-electrode glass cell with the RRDE system.

spinel $LiMn_2O_4$, acetylene black, and SFG-6 were first added to a solution of PVDF in *n*-methyl-2-pyrrolidone (NMP, Riedel-deHaen). The mixture is stirred for 20 min at room temperature with a magnetic bar, and then with a turbine for 5 min at 2000 rpm to make a slurry having the appropriate viscosity. The resulting slurry was coated onto a 6 mm diam stainless steel disk and dried at 120°C for 40 min. The resulting coating had a thickness of ~100 μm and an active material mass of ~2.4 mg. The quantity of active materials on the disk electrodes was kept constant (±0.2 mg) The disk electrodes were dried overnight at 100°C under vacuum before being transferred to an argon-filled glove box for cell assembly.

Electrochemical and ring-disk collection experiments.—The RRDE system (AFMT134DCPTT, Pine Instruments) with interchangeable disk consists of a 6 mm diam stainless steel disk electrode and a Pt ring electrode (1 mm width) with a 0.5 mm gap between them. The collection efficiency with this geometry is 0.24. The rotating ring-disk assembly was operated on a Pine AFMSRX rotator and CH705 Bipotentiostat (CH Instruments) with computerized interface. Experiments were conducted using the spinel $LiMn_2O_4$-containing disk electrodes and the dissolved Mn^{2+} from the disk was collected at the Pt ring. Lithium foil (Aldrich) was used as the reference and counter electrode. Figure 1 shows the schematic of a glass beaker cell with the RRDE system. A solution of $LiPF_6$ (1.0 M) in a 1:1 (v/v) mixture of ethylene carbonate (EC) and dimethyl carbonate (DMC) was used as the electrolyte (Ferro Corp.). A glass beaker cell, filled with 10 mL electrolyte, was used for electrochemical cycling and Mn^{2+} ion collection experiments. For the quantitative analysis of dissolved Mn^{2+} and the redox potential of $Mn^{2+}/Mn_{(s)}$ in the electrolyte solution, standards were prepared by dissolving anhydrous $MnCl_2$ (Aldrich) into the electrolyte solution or EC/DMC solvent. During the test, the spinel $LiMn_2O_4$-containing disk electrode potential was swept between 3.0 and 4.5 V *vs.* Li/Li^+ at 10 mV/s. While the Pt ring electrode was held at 1.0 V *vs.* Li. The Li anode was isolated from the cathode by two layers of Celgard 3401 separator and the Li reference electrode by a Vycor tip to avoid dissolved Mn ions deposited on the Li anode and reference electrode. The RDCE experiments consisted of the following sequential steps: (*i*) the $LiMn_2O_4$ disk was cycled at 10 mV/s with various voltage limits and temperatures at a fixed rotation speed, (*ii*) the Mn dissolved in the electrolyte during the cycling was collected for 30 min, and (*iii*) the collected reduction products were stripped from the ring. Stripping voltammograms (SVs) were collected by sweeping the ring potential from 0.8 to 2.8 V at 10 mV/s. For the *in situ* cell test, the spinel $LiMn_2O_4$ disk was cycled at 100 mV/s between 3.0 and 4.5 V or an extended voltage range at various conditions while the ring was held at 1.0 V to collect the Mn^{2+} ions generated from the disk electrode. Three tests were carried out for each con-

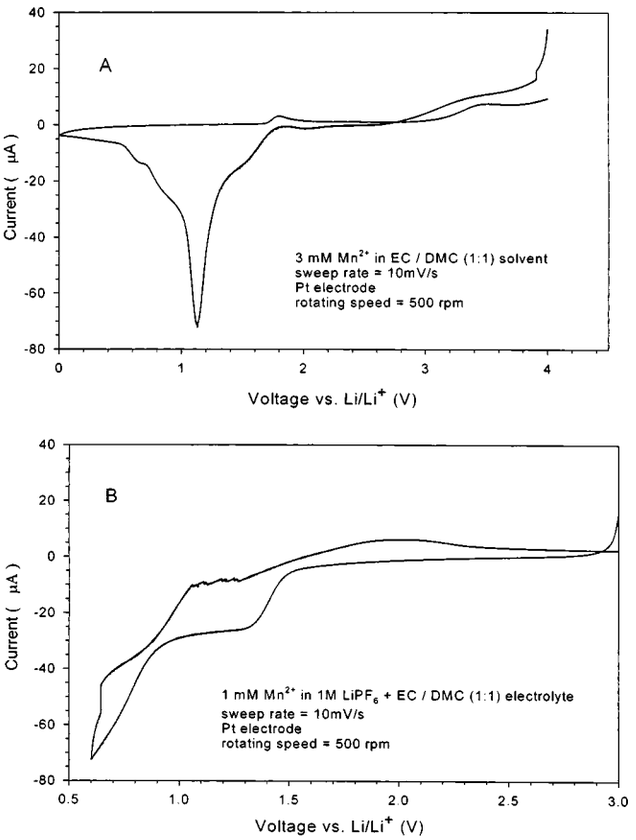

Figure 2. Cyclic voltammograms of Mn^{2+} ion. (A) 3 mM Mn^{2+} in EC/DMC (1:1) organic solvent cycled between 4.0 and 0.0 V at 10 mV/s and 500 rpm; (B) 1 mM Mn^{2+} in 1 M $LiPF_6$ + EC/DMC (1:1) electrolyte cycled between 3.0 and 0.6 V at 10 mV/s and 500 rpm.

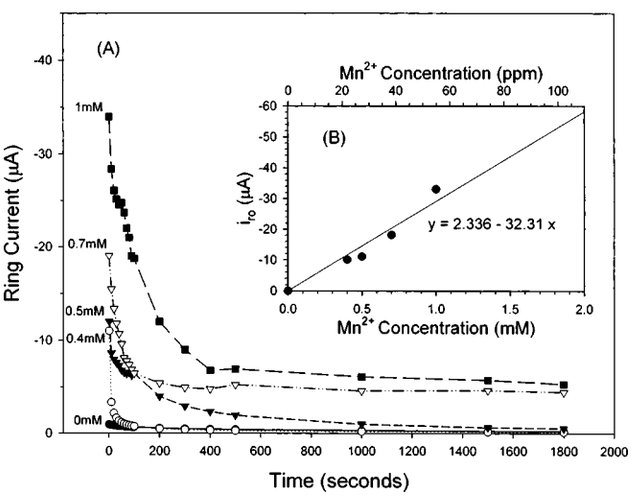

Figure 3. (A) The variation of ring current with time for standard Mn^{2+} ion concentrations at 0 (blank without Mn^{2+} ion), 0.4, 0.5, 0.7, and 1 mM; (B) Initial ring current (i_{r0}) *vs.* standard Mn^{2+} ion concentrations, based on 0 mM as $i_{r0} = 0$.

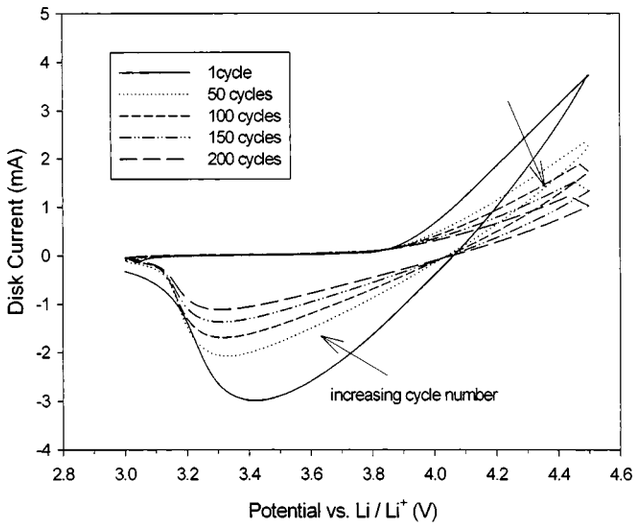

Figure 4. Cyclic voltammogram of representative spinel $LiMn_2O_4$ disk electrode in the beaker cell cycled between 3.0 and 4.5 V at 10 mV/s and 500 rpm with 1 M $LiPF_6$ + EC/DMC (1:1) electrolyte at 1, 50, 100, 150, and 200 cycles in room temperature.

dition, and the average performance was reported. In order to verify the dissolved Mn^{2+} ions in the electrolytes, some measurements on the concentrations of Mn^{2+} ions were also analyzed in ICP-MS (Perkin Elmer, SCIEX ELAN 5000). The cell fabrication and all measurements were carried out in a glove box filled with dry argon.

Results and Discussion

$Mn^{2+}/Mn_{(s)}$ vs. Li/L^+ redox potential.—The standard redox potential of $Mn^{2+}/Mn_{(s)}$ is 1.87 V *vs.* Li/Li^+. Cyclic voltammograms of 3 mM Mn^{2+} [in EC/DMC (1:1) solvent] and 1 mM Mn^{2+} (in 1 M LiPF+EC/DMC electrolyte) cycled between 4.0 and 0.0 V at 10 mV/s and 1000 rpm are shown in Fig. 2a and b, respectively. The reduction potential for Mn^{2+} is ~1.8 and ~1.58 V in the organic solvent and electrolyte, respectively. Li^+ ions are reduced below

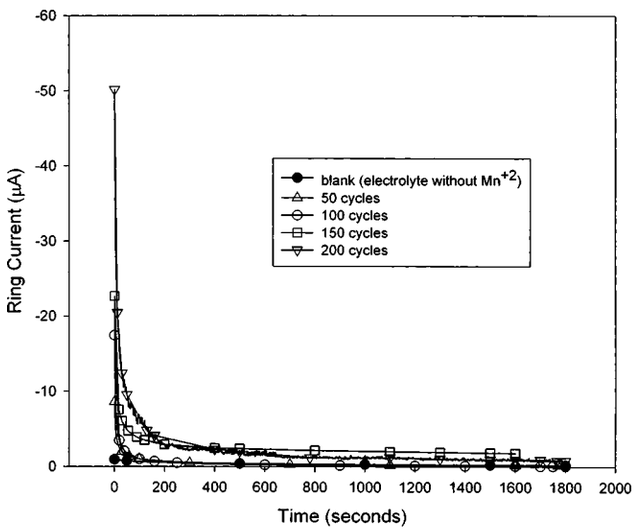

Figure 5. The variation of ring current with time for collection experiments conducted under the room temperature (~30°C) at various cycle numbers of spinel $LiMn_2O_4$ disk electrode sweeping linearly between 3.0 and 4.5 V at 10 mV/s and 500 rpm.

Table I. Concentrations of dissolved Mn^{2+} ions at various cycle numbers from the RRDEs and ICP-MS analysis results.[a]

Cycle no.	Dissolved Mn^{2+} ion concentration by RRDEs (mM)	Dissolved Mn^{2+} ion concentration by ICP-MS (mM)
50	0.31	0.28
100	0.58	-
150	0.75	0.81
200	1.6	1.52

[a] Based on 2.4 mg spinel $LiMn_2O_4$ disk electrodes with 86 wt % $LiMn_2O_4$ at room temperature.

~0.5 V in the electrolyte.[20] A ring potential of 1.0 V was chosen for the collection experiments to avoid the Li^+ ions reduction on the ring electrode.

In this study, $Mn^{2+}/Mn_{(s)}$ potential step chronoamperometry on the ring electrode was used to measure the dissolved Mn ion concentration in the electrolyte solution. Figure 3a shows the variation of ring current with time for standard Mn^{2+} ion concentration in the electrolyte at 0 (blank without Mn^{2+} ion), 0.4, 0.5, 0.7, 1 mM. The potential of the ring electrode was stepped from open to 1.0 V while rotating at 500 rpm. In Fig. 3a, the initially recorded ring current (i_{r0}) is at its maximum and is proportional to the initial Mn^{2+} ion concentration in the solution, as displayed in Fig. 3b. Since the relationship between concentration *vs.* the initial ring current shows a good linearity for i_{r0} from 0.4 to 1 mM of Mn^{2+} ion concentration, it can be concluded that the dissolved Mn^{2+} concentrations in the electrolytes can be analyzed successfully by potential step chronoamperometry.

Cycle number effects on spinel dissolution.—The cyclic voltammograms for our spinel electrode cycled at room temperature (~30°C) between 4.5 and 3.0 V are shown in Fig. 4. The spinel disk electrodes, which initially lose capacity rapidly with cycling, eventually, after about 50 cycles, begin to exhibit capacity retention with cycling as good as the best spinels. Capacities of the spinels were calculated from the cyclic voltammograms and exhibited the initial capacity of only 26 mAh/g in the first discharge. Only a fraction of the actual capacity is accessible at this high sweep rate. The discharge capacity declined to less than 10 mAh/g by the end of 200 high-rate cycles. The loss in capacity is 0.87% per cycle before 50 cycles and then, about 0.35% per cycle loss until 200 cycles. The

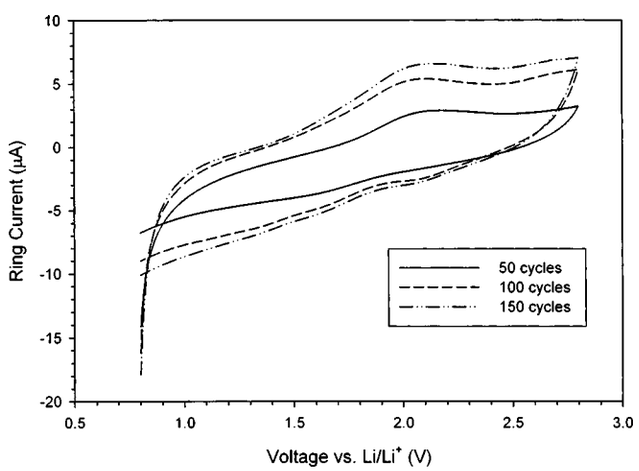

Figure 6. Stripping voltammograms were conducted from the collected $Mn_{(s)}$ on the ring electrode in this figure by sweeping the potential from 0.8 to 2.8 V at 10 mV/s.

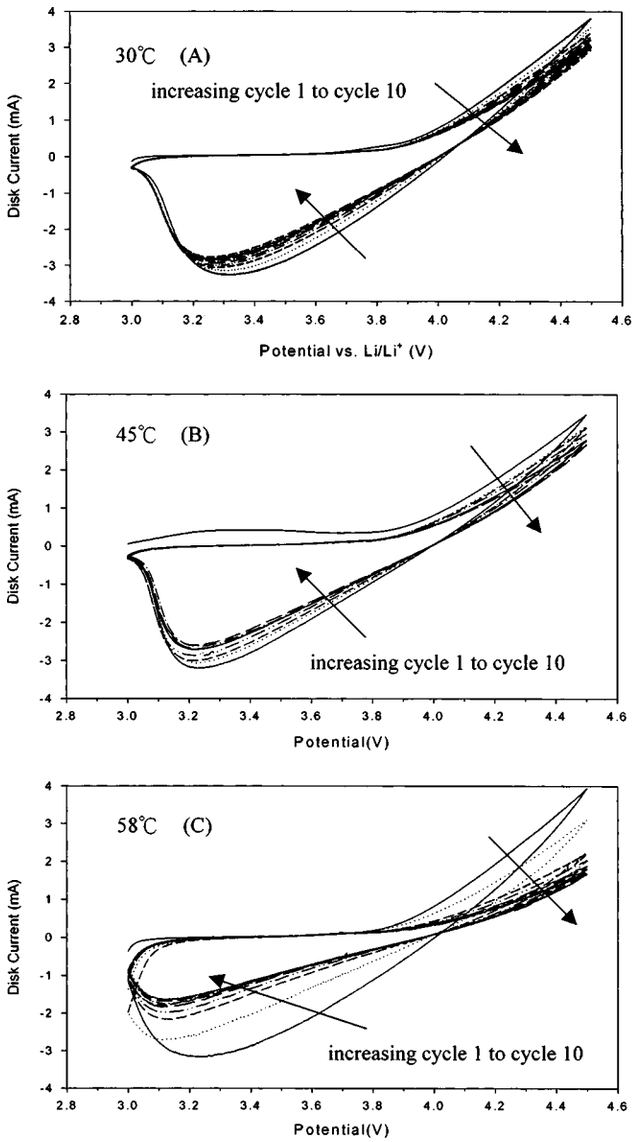

Figure 7. Cyclic voltammograms of three spinel $LiMn_2O_4$ disk electrodes in the beaker cell cycled between 3.0 and 4.5 V at 10 mV/s and 500 rpm with 1 M $LiPF_6$ + EC/DMC (1:1) electrolyte at (A) 30, (B) 45, and (C) 58°C.

dissolved Mn ion in the electrolyte was measured during the cycling. The variation of ring current with time is shown in Fig. 5 for collection experiments conducted at room temperature at various cycle numbers of spinel $LiMn_2O_4$ disk electrode sweeping linearly between 3.0 and 4.5 V at 10 mV/s and 500 rpm. It is obvious that the initial ring current increases with cycle number. The concentrations of dissolved Mn^{2+} ions in the electrolytes were estimated from the correlation in Fig. 3. These measurements, along with comparisons between the RRCEs and ICP-MS analysis methods for some concentrations of dissolved Mn^{2+} ions are shown in Table I. The values of Mn^{2+} concentration agree well. These results showed the dissolved Mn^{2+} ion concentration of 0.31 mM after 50 cycles at room temperature. As the disk electrode was cycled, more Mn was detected in the electrolyte. The rate of the Mn dissolution was fairly constant up to 150 cycles, and then it appeared to accelerate. According to the experimental data from Table I, the average dissolved Mn^{2+} ion concentration was about 0.44% for each cycle before 150 cycles and then increased rapidly to 1.63% per cycle by the end of

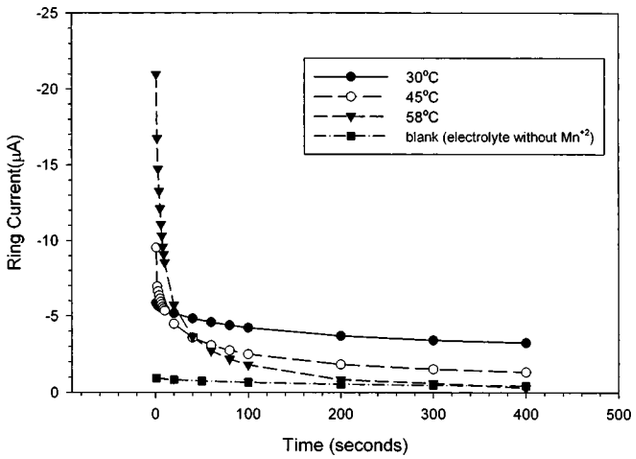

Figure 8. The variation of ring current with time for collection experiments conducted under various temperature (30, 45, and 58°C) after 10 cycles of spinel $LiMn_2O_4$ disk electrode sweeping linearly between 3.0 and 4.5 V at 10 mV/s and 500 rpm.

200 cycles. The amount of dissolved Mn at 200 cycles is about 2.75 times as large as that at 100 cycles as shown in Table I. Therefore, the Mn dissolution was accelerated for higher cycle number. A similar dissolution tendency was reported by Terada *et al.*[18] In Fig. 4, the rapid capacity fading initially is not caused only by the simple dissolution of Mn since the Mn dissolution rate is almost constant before 150 cycles. Another possibility for capacity fading originates from the structural change and electrolyte decomposition.[8] Figure 6 exhibits the stripping voltammograms conducted from the collected $Mn_{(s)}$ on the ring electrode in Fig. 5 by sweeping the potential from 0.8 to 2.8 V at 10 mV/s. Only one peak, centered at +2.0 V in Fig. 6, is due to the oxidative formation of Mn^{2+} from $Mn_{(s)}$. in Fig. 2b.

Elevated temperature effects on spinel dissolution.—Many investigations[8,14,18-23] have shown that the dissolution of Mn was accelerated at elevated temperatures leading to a faster capacity fading. Plots of the cyclic voltammogram of three spinel $LiMn_2O_4$ disk electrodes in the beaker cell cycled between 3.0 and 4.5 V with 10 mV/s, 500 rpm, and 1 M $LiPF_6$ + EC/DMC (1:1) electrolyte, at 30, 45, and 58°C are shown in Fig. 7. The initial discharge capacities were 26, 25.5, and 27.8 mAh/g at 30, 45, and 58°C, respectively. The capacity for spinel $LiMn_2O_4$ disk electrode decreased slowly at room temperature by about 2.1% per cycle in the first 10 cycles as

Table II. Concentrations of dissolved Mn^{2+} ions at various cycle conditions from the RRDEs analysis results.[a]

Experimental conditions (after 100 cycles)	Dissolved Mn^{2+} ion concentration (mM)
Effect of overdischarge	
Disk scan between 2.7 and 4.1 V	1.06
Disk scan between 3.0 and 4.1 V	0.36
Disk scan between 3.4 and 4.1 V	0.13
Effect of overcharge	
Disk scan between 3.4 and 4.3 V	0.27
Disk scan between 3.4 and 4.5 V	0.39
Disk scan between 3.4 and 4.8 V	0.84
Effect of rotation speed (rpm)	
500	0.56
1000	0.61
2000	0.62

[a] Based on 2.4 mg spinel $LiMn_2O_4$ disk electrodes with 86 wt % $LiMn_2O_4$ at room temperature.

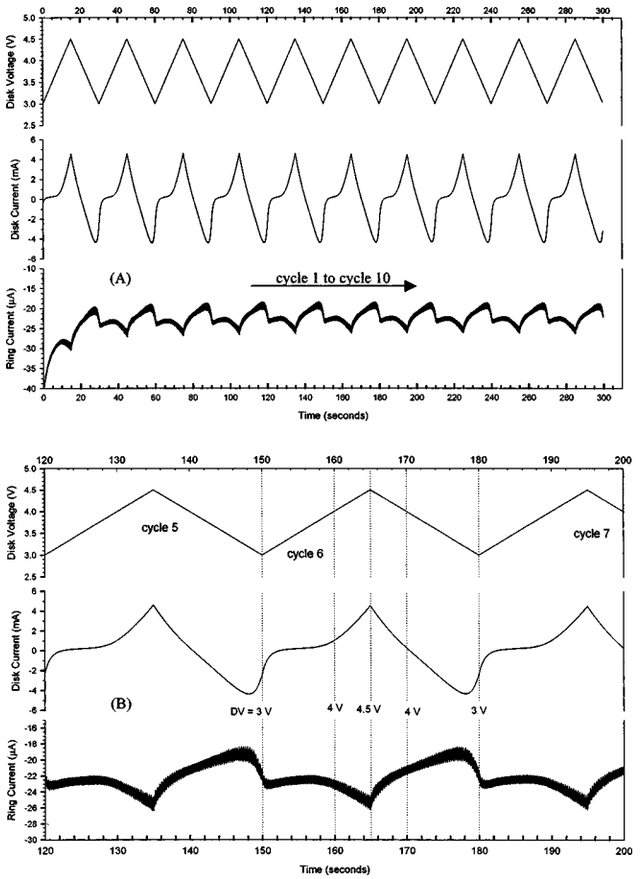

Figure 9. RRDE profiles for Mn^{+2} collection experiments conducted under room temperature and 1000 rpm at spinel $LiMn_2O_4$ disk electrode cycled between 3.0 and 4.5 V at 100 mV/s and ring electrode held at 1.0 V in 1 M $LiPF_6$ + EC/DMC (1:1) electrolyte: (A) cycle 1 to cycle 10, (B) cycle 5, 6, and 7.

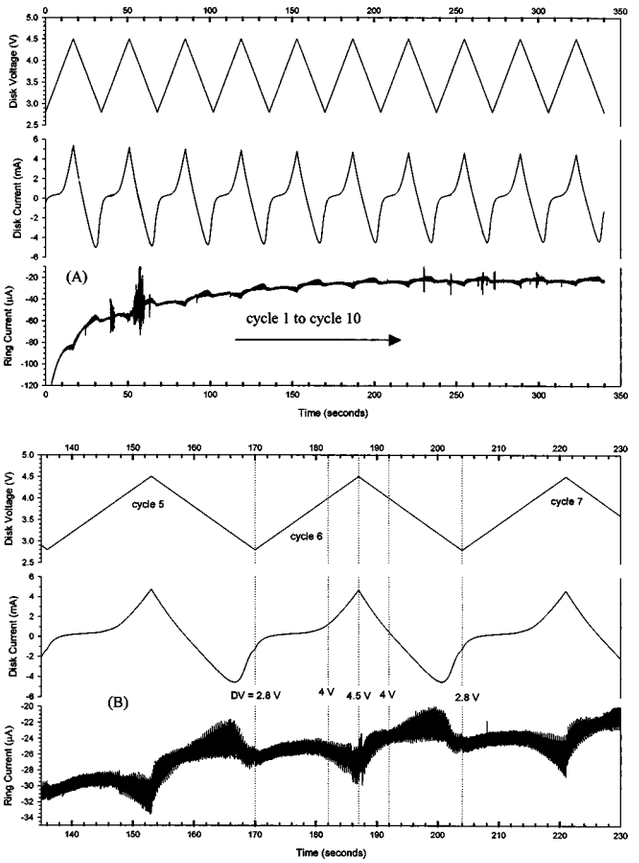

Figure 10. RRDE profiles for Mn^{+2} collection experiments conducted under 53°C and 1000 rpm at spinel $LiMn_2O_4$ disk electrode cycled between 2.8 and 4.5 V at 100 mV/s and ring electrode held at 1.0 V in 1 M $LiPF_6$ + EC/DMC (1:1) electrolyte: (A) cycle 1 to cycle 10, (B) cycle 5, 6, and 7.

shown in Fig. 7a. In Fig. 7b, the capacity-loss rate was about 3.0% per cycle during cycling at 45°C. When the temperature was increased to 58°C, as shown in Fig. 7c, the initial capacity was slightly higher, but the capacity faded much faster at about 7.8% per cycle. The capacitance-voltage (C-V) experimental results indicated that the capacities faded faster at elevated temperatures. Figure 8 shows the variation of ring current with time for collection experiments conducted at various temperatures (30, 45, and 58°C) after 10 cycles between 3.0 and 4.5 V at 10 mV/s and 500 rpm. In Fig. 8, the larger initial ring current at a higher temperature indicates that the amount of Mn dissolution increases with elevated temperature. The concentrations of dissolved Mn were evaluated to be 0.22, 0.33, and 0.69 mM at 30, 45, and 58°C, respectively. The amount of dissolved Mn at 58°C is about three times as large as that at 30°C after the initial 10 cycles. The experimental results demonstrates that dissolution of Mn was accelerated at elevated temperatures above 45°C, in agreement with the literature.[8,18] Figure 7 and 8 show that the data exhibiting the capacity fading is definitely coincident with Mn dissolution at elevated temperatures.

Effect of overdischarge, overcharge, and rotation speed.—Several collection experiments were carried out to study the effects of overcharge, overdischarge, and rotation speed. The amounts of Mn dissolution after 100 cycles under various conditions are summarized in Table II. The results show that manganese dissolution increases upon decreasing the lower voltage limit. As the spinel electrode discharges the Mn^{3+} content in the spinel electrode increases. The large increase of the Mn^{3+}-rich $Li_2Mn_2O_4$ phase at overdischarge to 2.7 V caused the concentration of Mn increase rapidly as shown in Table II. The equilibrium potential for $Li_2Mn_2O_4$ formation is below 3 V, but it has been detected above 3 V,[24] the presence of tetragonal $Li_2Mn_2O_4$ on the surface is increased at the discharge of spinel $LiMn_2O_4$ electrode below 3 V. The study of the effect of overcharge on the Mn dissolution also exhibited larger rates of Mn dissolution as the charged voltage is increased, as shown in Table II. The concentration is increased rapidly as the electrode overcharges to 4.8 V. The amounts of Mn dissolution increase at the higher charged voltage can be attributed to the formation of instability in the delithiated structure at the top charged state which losses MnO through dissolution of Mn to a more stable single-phase structure.[4,8,9] Table II also shows that the concentrations of Mn detected were independent of the speed of rotation, which suggests that Mn dissolution from the disk electrode was under kinetic control, in agreement with the literature.[19]

In situ measurements of Mn dissolution during cycling.—The *in situ* monitoring of Mn dissolution from the spinel $LiMn_2O_4$ electrode was carried out during cycling voltammetry or galvanostatic charge and discharge by means of the RRDE collection experiments. Figure 9a shows both the disk and ring current profiles for the first 10 cycles of the spinel electrode between 3.0 and 4.5 V with a sweep rate of 100 mV/s and room temperature. The ring electrode was held at 1.0 V, and the rotation speed was 1000 rpm. The disk anodic and cathodic currents corresponding to charge and discharge were stable over the first 10 cycles. In conjunction with the disk electrode, a regular shape of the ring current was observed after the first cycle as

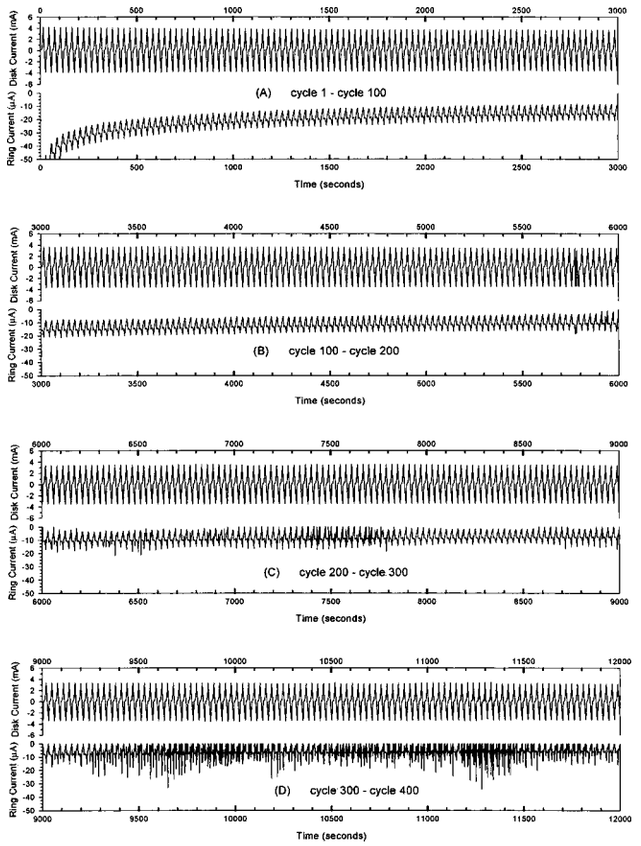

Figure 11. RRDE profiles for Mn^{+2} collection experiments conducted under room temperature and 1000 rpm at spinel $LiMn_2O_4$ disk electrode cycled between 3.0 and 4.5 V at 100 mV/s and ring electrode held at 1.0 V in 1 M $LiPF_6$ + EC/DMC (1:1) electrolyte: (A) cycle 1 to cycle 100, (B) cycle 100 to cycle 200, (C) cycle 200 to cycle 300, (D) cycle 300 to cycle 400.

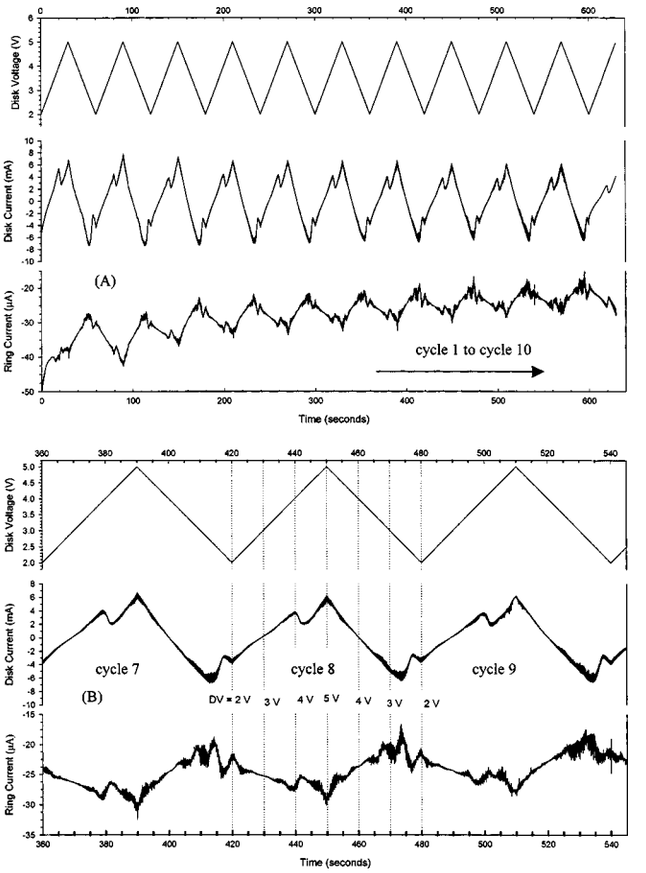

Figure 12. RRDE profiles for Mn^{+2} collection experiments conducted at room temperature and 1000 rpm at spinel $LiMn_2O_4$ disk electrode cycled between 2.0 and 5.0 V at 100 mV/s and ring electrode held at 1.0 V in 1 M $LiPF_6$ + EC/DMC (1:1) electrolyte: (A) cycle 1 to cycle 10; (B) cycle 7, 8, and 9.

shown in Fig. 9a. The ring cathodic peak current indicated that some Mn atoms dissolved from the disk electrode into the electrolyte solution, forming soluble oxidized Mn^{+2} ion species that were reduced on the ring electrode. In all of the *in situ* studies, the first cycle exhibited a larger ring cathodic current due to the fresh Pt ring more active for Mn^{+2} deposition. Figure 9b shows expended RRDE profiles for cycles 5, 6, and 7. Obviously, the ring cathodic current increased from about 3.5 V (disk potential) and became noticeable at potentials above 4.0 V and then reached a maximum when the disk potential went up to 4.5 V during the charged process. On the cathodic sweep, the ring cathodic current became noticeable at a potential below 3.1 V (disk potential) and reached a maximum when the disk potential dropped to 3.0 V. The ring currents exhibited maxima corresponding to the end-of-charge (EOC) and end-of-discharge (EOD), with the largest peak at the EOC. These results suggest that dissolution of Mn from spinel $LiMn_2O_4$ is the highest at voltage end points, with most of the Mn dissolution occurring at the EOC. This is in good agreement with most of the evidence reported thus far which points to solubility at the top of charge as the major reason for the capacity fade in $Li/Li_x[Mn_2]O_4$ cells.

The effect of elevated temperature and overdischarge of the spinel electrode with the RRDE profiles is shown in Fig. 10a and b. Figure 10a shows the disk and ring current profiles for the first 10 cycles when the spinel $LiMn_2O_4$ electrode was scanned between 2.8 and 4.5 V at 100 mV/s at 53°C. The shape of both disk and ring currents in Fig. 10a was similar to that in Fig. 9a. Both had two maximum ring currents appearing in the same region of the disk potential. However, the ring cathodic currents in Fig. 10b are larger than those in Fig. 9b, as expected at higher temperatures. It is clear that the dissolution of the Mn rate is increased at elevated temperatures. This result is in good agreement with those in Fig. 8. The first five cycles exhibited a larger ring cathodic current decay due to the ring's greater activity at high temperature for Mn collection.

For the room temperature experiment, cycles were continued up to 400 cycles as shown in Fig. 11. The first 30 cycles exhibited a larger ring cathodic current decay due to the ring's greater activity for the Mn collection. The shape of the profiles was steady up to about 320 cycles, and the maximum ring cathodic currents decreased slowly after which the ring cathodic currents became irregular. The slow decrease of the maximum ring cathodic currents is attributed to the occupation of the reduced Mn on the Pt ring surface causing the ring to be less active for Mn collection.

In order to study the *in situ* monitoring of Mn dissolution during overcharge and overdischarge, the RRDE profile was examined between 2.0 and 5.0 V. Figure 12 shows the disk and ring current profiles for the first 10 cycles of the spinel $LiMn_2O_4$ electrode were scanned between 2.0 and 5.0 V at 100 mV/s. With this wide voltage window, the disk currents for charge and discharge decreased significantly indicating rapid capacity fade, as discussed above. In conjunction with the disk electrode under charge and discharge, a regular shape of the ring current was observed after the first cycle in Fig. 12a. Figure 12b shows the expanded RRDE profiles for cycles 7, 8, and 9. It is obvious that seven ring current maxima are observed in this voltage range. The first three peaks occur at disk potentials of 2.3, 3.9, and 5.0 V on the anodic sweep and the other four peak

occur at 4.5, 3.5, 2.9, and 2.3 V on the cathodic sweep. These observations suggest that the dissolution of Mn from spinel $LiMn_2O_4$ occurs during the charged process, followed by the discharged process. From the experimental results, the Mn dissolution from the spinel $LiMn_2O_4$ electrode occurred at the end of the charged and discharged steps, and especially, at the top of the charged stage, the Mn dissolution was accelerated causing capacity fading. A similar dissolution tendency has been noted in many reports.[4,7-11]

Conclusion

Mn dissolution from a thin porous spinel $LiMn_2O_4$ electrode was measured with rotating ring-disk collection experiments. During room temperature cycling in the normal voltage window for $LiMn_2O_4$, Mn concentrations increased linearly with cycle number correlated to capacity loss from the spinel up to 150 cycles. After 150 cycles, the Mn dissolution rate was accelerated. From the study of collection experiments at 30, 45, and 58°C, the amount of dissolved Mn at 58°C is about three times as large as that at 30°C after 10 cycles. The concentrations of dissolved Mn in the electrolyte were increased when the disk electrodes were overcharged and overdischarged, suggesting that the acceleration of the Mn dissolution occurred during these processes. However, the detection of dissolved Mn was independent of the rotation speed of the disk, which indicated the Mn dissolution from the disk as well as Mn^{2+} reduction on the ring were under reaction control.

The *in situ* monitoring of Mn dissolution from the spinel $LiMn_2O_4$ electrode was carried out under various conditions. The ring currents exhibited maxima corresponding to the EOC and EOD, with the largest peak at the EOC. The results show that dissolution of Mn from spinel $LiMn_2O_4$ occurs during charge/discharge cycling, especially in a charged state (at >4.1 V) and in a discharged state (at <3.1 V). The larger peak at EOC demonstrated that Mn dissolution took place mainly at the top of charge. At elevated temperatures, the ring cathodic currents were also larger due to the increase of the Mn dissolution rate.

Acknowledgments

The authors thank the National Science Council of Taiwan for the financial support in this work under contract no. NSC-89-2214-E-214-011. The authors also thank Forex Pro Enterprise Co. (Taiwan) for providing useful materials.

I-Shou University assisted in meeting the publication costs of this article.

References

1. Y. Nishi, *J. Power Sources*, **100**, 101 (2001).
2. G. Pistoia, A. Antonini, R. Rosati, and D. Zane, *Electrochim. Acta*, **41**, 2683 (1996).
3. A. Antonini, C. Bellitto, M. Pasquali, and G. Pistoia, *J. Electrochem. Soc.*, **145**, 2726 (1998).
4. D. H. Jang, Y. J. Shin, and S. M. Oh, *J. Electrochem. Soc.*, **143**, 2204 (1996).
5. R. J. Gummow, A. de Kock, and M. M. Tackeray, *Solid State Ionics*, **69**, 59 (1994).
6. E. Wang, D. Ofer, W. Bowden, N. Iltchev, R. Moses, and K. Brandt, *J. Electrochem. Soc.*, **147**, 4023 (2000).
7. T. Aoshima, K. Okahara, C. Kiyohara, and K. Shizuka, *J. Power Sources*, **97-98**, 377 (2001).
8. Y. Xia, Y. Zhou, and M. Yoshio, *J. Electrochem. Soc.*, **144**, 2593 (1997).
9. A. Yamada, K. Miura, K. Hinokuma, and M. Tanaka, *J. Electrochem. Soc.*, **142**, 2149 (1995).
10. M. M. Thackeray, *J. Electrochem. Soc.*, **142**, 2558 (1995).
11. G. Pistoia and G. Wang, *Solid State Ionics*, **66**, 135 (1993).
12. Y. Gao and J. R. Dahn, *J. Electrochem. Soc.*, **143**, 100 (1996).
13. J. M. Tarascon, F. Coowar, G. Amatucci, F. K. Shokoohi, and D. Guyomard, *J. Electrochem. Soc.*, **141**, 1421 (1994).
14. Y. J. Shin and A. Manthiram, *Electrochem. Solid-State Lett.*, **5**, A55 (2002).
15. H. Huang, C. A. Vincent, and P. G. Bruce, *J. Electrochem. Soc.*, **146**, 3649 (1999).
16. D. H. Jang, Y. J. Shin, and S. M. Oh, *J. Electrochem. Soc.*, **144**, 3342 (1997).
17. Y. Xia and M. Yoshio, *J. Power Sources*, **66**, 129 (1997).
18. Y. Terada, Y. Nishiwaki, I. Nakai, and F. Nishikawa, *J. Power Sources*, **97-98**, 420 (2001).
19. A. D. Pasquier, A. B. Courjal, D. Larcher, G. Amatucci, B. Gerand, and J. M. Tarascon, *J. Electrochem. Soc.*, **146**, 428 (1999).
20. X. Zhang, R. Kostecki, T. J. Richardson, J. K. Pugh, and P. N. Ross, *J. Electrochem. Soc.*, **148**, A1341 (2001).
21. M. Thackeray, S. H. Yang, A. Kahaian, K. D. Kepler, E. Skinner, J. Vaughey, and S. Hackney, *Electrochem. Solid-State Lett.*, **1**, 7 (1998).
22. H. Yamane, T. Inoue, M. Fujita, and M. Sano, *J. Power Sources*, **99**, 60 (2001).
23. G. G. Amatucci, N. Pereira, T. Zheng, and J.-M. Tarascon, *J. Electrochem. Soc.*, **148**, 171 (2001).
24. K. A. Striebel, E. Sakai, and E. J. Cairns, *J. Electrochem. Soc.*, **149**, A61 (2002).